

Electron acceleration in downward auroral field-aligned currents

Alexandra P. Cran-McGreehin and Andrew N. Wright

Mathematical Institute, University of St. Andrews, St. Andrews, Fife, UK

Received 11 November 2004; revised 4 May 2005; accepted 16 May 2005; published 29 September 2005.

[1] The auroral downward field-aligned current is mainly carried by electrons accelerated up from the ionosphere into the magnetosphere along magnetic field lines. Current densities are typically of the order of a few $\mu\text{ Am}^{-2}$, and the associated electrons are accelerated to energies of several hundred eV up to a few keV. This downward current has been modeled by Temerin and Carlson (1998) using an electron fluid. This paper extends that model by describing the electron populations via distribution functions and modeling all of the F region. We assume a given ion density profile, and invoke quasi-neutrality to solve for the potential along the field line. Several important locations and quantities emerge from this model: the ionospheric trapping point, below which the ionospheric population is trapped by an ambipolar electric field; the location of maximum E_{\parallel} , of the order of a few mVm^{-1} , which lies earthward of the B/n peak; the acceleration region, located around the B/n peak, which normally extends between altitudes of 500 and 3000 km; and the total potential increase along the field line, of the order of a few hundred V up to several kV. The B/n peak is found to be the central factor determining the altitude and magnitude of the accelerating potential required. Indeed, the total potential drop is found to depend solely on the equilibrium properties in the immediate vicinity of the B/n peak.

Citation: Cran-McGreehin, A. P., and A. N. Wright (2005), Electron acceleration in downward auroral field-aligned currents, *J. Geophys. Res.*, 110, A10S15, doi:10.1029/2004JA010898.

1. Introduction

[2] Field-aligned currents (FACs) are a common feature of space plasmas, their main role being to couple two different regions of plasma by carrying current between them along magnetic field lines. In the Jovian system, FACs couple Jupiter with Io and the Jovian magnetodisc. FACs also flow along Earth's auroral magnetic field lines, coupling the cold, dense ionosphere with the hot, tenuous magnetosphere. Upward FACs are carried by accelerated downflowing electron beams, and interest in these currents was originally piqued by their remarkable visible manifestation, the aurora. The FACs flowing around the Earth are easily observable, and give us insight into basic plasma processes such as particle energization and instabilities. There have been many observations of the downflowing electron beams supported by large inverted-V converging electric field structures. Until recently, however, there had only been sporadic evidence for the existence of upflowing electron beams by satellites and rockets including Viking and FREJA [Marklund *et al.*, 1994]. In 1996, the Fast Auroral SnapshoT (FAST) satellite was launched, and it has proved to be very successful in identifying downward current regions. The diverging electric field structures and upflowing electron beams associated with the downward current region tend to exist at the edge of upward current regions, and are much narrower in latitude. FAST's im-

proved time resolution and continuous observance of all pitch angles have enabled observers to analyze these regions, and data have shown that upflowing electron beams occur just as frequently as their downward counterparts.

[3] Studies of FAST observations of the downward current region by Carlson *et al.* [1998], Ergun *et al.* [1998] and Elphic *et al.* [2000] all indicate correlated increases in electron energy and potential (inferred from $\int \mathbf{E} \cdot d\mathbf{s}$), which suggest stability of the potential structures at least on the electron acceleration timescale. These results support the theory that the electrons are energized by quasi-static parallel potential structures, and we have used this idea to formulate a simple overview of the main features of the downward current region. The observational studies, including Andersson *et al.* [2002], also indicate that many complex and small-scale features may sometimes occur in this region: the narrow accelerating potential may extend for ~ 10 Debye lengths, followed by a similarly small region where the accelerated beam can be observed. This beam is unstable, and is rapidly stabilized thereafter by strong wave turbulence and electron phase-space holes. Also, although one might expect ions to be accelerated downward by this electric field structure, observations point to the existence of ion conics earthward of the potential structure, which are trapped between their mirror point and this potential. Statistical studies of the downward current region reveal that the upward beams occur most often in the winter hemisphere, pointing to the ion scale height and number density as the key factors determining the nature of the required acceleration [Cattell *et al.*, 2004].

[4] The single fluid Magnetohydrodynamic (MHD) approximation, successful in many applications related to large-scale current systems, is not suitable for modeling all aspects of FACs since this limit neglects electron mass compared with that of the ions. FACs are mainly carried by electrons accelerated to energies of \sim keV: MHD cannot describe the nature of this energization since massless electrons are infinitely mobile and move to wherever they are needed to carry any required current. Hence another approach is needed. Quasi-neutrality has been a primary modeling constraint for some time: *Chiu and Schultz* [1978] and *Stern* [1981] both considered the generation of parallel electric fields along an auroral field line embedded in a cold, dense ionosphere near the Earth, and a hot, tenuous magnetosphere further away. *Chiu and Schultz* [1978] examined upward currents, and found potential differences of the order of 1 kV; in their examples, E_{\parallel} maximized at an altitude of 2000–2500 km and extended to $\sim 1 R_E$. *Stern's* [1981] model produced double layers (discontinuities which can evolve due to the different plasma properties of the ionosphere and magnetosphere) for equilibria and upward and downward currents. More recently, *Ergun et al.* [2000], *Rönmark* [2002], *Vedin and Rönmark* [2004] and *Wright and Hood* [2003] have all modeled the upward current region.

[5] Less attention has focused on modeling the downward current region. *Temerin and Carlson* [1998] present an ionospheric electron fluid model with fixed ion density, using quasi-neutrality to constrain the solution and obtain the required parallel potential drop. They obtain parallel potential drops of several kV for current densities of a few μ Am $^{-2}$. *Jasperse* [1998] uses a Vlasov model incorporating ion heating and wave effects, which explains the production of upward field-aligned electron beams, downward pointing parallel electric fields and ion conics.

[6] The model presented here extends the work of *Temerin and Carlson* [1998] via the use of electron distribution functions. We also model the entire F region, enabling us to predict the height at which the beam emerges from the ionosphere, and the extent of the energization region.

2. Model

[7] Following the approach of *Wright and Hood* [2003] in their model of the upward current region, we consider a one-dimensional Vlasov model of the motion of upward accelerated electrons on an auroral field line within a few R_E of the Earth. We find the steady solution for the downward current region by setting $\partial/\partial t = 0$, and model the equilibrium magnetic field, \mathbf{B} , as being locally dipolar in the acceleration region, giving

$$B = \frac{B_0 \sqrt{1 + 3 \sin^2 \theta}}{\cos^6 \theta}, \quad (1)$$

where B_0 is a constant, θ is the latitude, and

$$r = LR_E \cos^2 \theta, \quad (2)$$

where r is the radial distance to a point on the field line. L is taken to be 10, giving an invariant latitude of 71.6° as the

field line enters the ionosphere. The arc length element along \mathbf{B} , $d\ell$, is given by

$$d\ell = d\theta \sqrt{r^2 + \left(\frac{dr}{d\theta}\right)^2} \quad (3)$$

[8] Using equations (3) and (2), we can see that the length along the field line, ℓ , which increases on approaching the ionosphere, is given by

$$\ell = \int_0^\theta LR_E \cos \theta \sqrt{1 + 3 \sin^2 \theta}, \quad (4)$$

which can be solved to give

$$\ell = \frac{LR_E}{2\sqrt{3}} \left(\frac{1}{2} \sinh \left(2 \sinh^{-1} \left(\sqrt{3} \sin \theta \right) \right) + \sinh^{-1} \left(\sqrt{3} \sin \theta \right) \right) \quad (5)$$

[9] This model extends from a distant point in the magnetosphere, ℓ_0 , whose exact location is not important, to the base of the F region, ℓ_m , taken to be at a radial distance of $1 R_E$. We model the acceleration region as having a dipole magnetic geometry, however, it is not necessary that the field line remains dipolar beyond this region. We impose a fixed ion density profile along the field line. Obviously, potential variation along the field line will affect the ions as well as the electrons; however, the ions are much heavier than the electrons, so we assume that their reaction is negligible, giving a short-timescale solution to the problem. We use an exponentially decaying number density of the form

$$n = n_0 + (n_m - n_0) \exp \left[-\frac{r - R_E}{h} \right], \quad (6)$$

where n_m and n_0 are the ion number densities at ℓ_m and ℓ_0 respectively, and h is the ion scale height. Assuming that the ions are singly charged and the plasma quasi-neutral, equation (6) also gives the total number density of the electron populations.

[10] In this paper, we take $B_0 = 25$ nT, giving B in the ionosphere of 5×10^4 nT, $n_0 = 10^6$ m $^{-3}$, $n_m = 10^{12}$ m $^{-3}$, and $h = 100$ km, unless stated otherwise. We show the variation of B/n with s in Figure 1, which has the characteristic single peak at an altitude of 1720 km, where s is the field-aligned coordinate measured from the ionospheric end given by $s = \ell_m - \ell$. Thus $s = 0$ at the base of the F region and increases with altitude.

[11] Following *Wright and Hood* [2003], we model the ionospheric electron population via a gyro-averaged distribution function $f_i(\ell, v_{\parallel}, v_{\perp}, t)$, where v_{\parallel} and v_{\perp} are the parallel and perpendicular components of the electron velocity, and t is time. This distribution function satisfies the general guiding center gyrotropic Vlasov equation,

$$\frac{\partial f}{\partial t} + \frac{\partial f}{\partial \ell} \frac{d\ell}{dt} + \frac{\partial f}{\partial v_{\parallel}} \frac{dv_{\parallel}}{dt} + \frac{\partial f}{\partial v_{\perp}} \frac{dv_{\perp}}{dt} = 0 \quad (7)$$

and we assume that the magnetic moment, $\mu = mv_{\perp}^2/2B$, is conserved on an electron trajectory. We seek a solution of the form

$$f_i = F(\ell, v_{\parallel}, v_{\perp}, t) g(\mu) \quad (8)$$

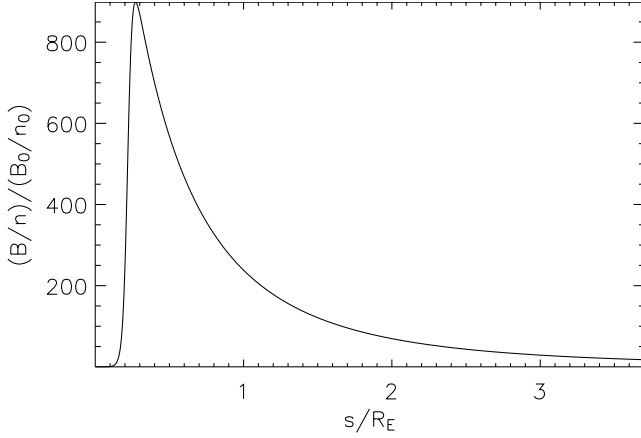


Figure 1. The variation of B/n , normalized by B_0/n_0 , along an $L = 10$ field line. The path length is measured from the base of the F-region ($s = \ell_m - \ell$). The B/n peak occurs at $s/R_E = 0.271$.

where $g(\mu)$ is an arbitrary function of μ . Since f_i and μ are both conserved on an electron trajectory, we can deduce that F is also conserved on an electron trajectory. Following *Wright and Hood* [2003], we substitute equation (8) into equation (7), using μ invariance and noting that $m(dv_{\parallel}/dt) = -eE_{\parallel} - \mu(\partial B/\partial \ell)$, and find that

$$0 = g(\mu) \left(\frac{\partial F}{\partial t} + v_{\parallel} \frac{\partial F}{\partial \ell} - \left(\frac{eE_{\parallel}}{m} + \frac{v_{\perp}^2}{2B} \frac{\partial B}{\partial \ell} \right) \frac{\partial F}{\partial v_{\parallel}} + \frac{v_{\parallel} v_{\perp}}{2B} \frac{\partial B}{\partial \ell} \frac{\partial F}{\partial v_{\perp}} \right) \quad (9)$$

[12] We take $g(\mu) = (m/\pi\bar{\mu})\delta(\mu/\bar{\mu})$, where δ is a standard delta function, and $\bar{\mu}$ is a normalizing constant, to focus on field-aligned motion since observations and μ conservation both give a highly collimated electron beam. We can integrate $g(\mu)$ over v_{\perp} space by multiplying by $2\pi v_{\perp} dv_{\perp}$, and integrating from $0 < v_{\perp} < \infty$ as follows:

$$\begin{aligned} \int_0^{\infty} g(\mu) 2\pi v_{\perp} dv_{\perp} &= \int_0^{\infty} \frac{m}{\pi\bar{\mu}} \delta\left(\frac{\mu}{\bar{\mu}}\right) 2\pi v_{\perp} dv_{\perp} \\ &= \int_0^{\infty} 2B\delta\left(\frac{\mu}{\bar{\mu}}\right) d\left(\frac{\mu}{\bar{\mu}}\right) \\ &= B \end{aligned} \quad (10)$$

[13] Using this result, we integrate equation (9) over v_{\perp} space in the same way to give

$$B \frac{\partial F}{\partial t} + v_{\parallel} B \frac{\partial F}{\partial \ell} - \frac{eE_{\parallel} B}{m} \frac{\partial F}{\partial v_{\parallel}} = 0 \quad (11)$$

and $F = F(\ell, v_{\parallel}, v_{\perp} = 0, t)$. F serves as a simplified distribution function for the ionospheric electrons and has units of $m^{-4} s T^{-1}$. Equation (11) shows how our assumption of small μ (implicit in the choice of g) means the mirror force is not important for the ionospheric electrons. In equation (9), the coefficient of $\partial F/\partial v_{\parallel}$ represents the parallel components of the \mathbf{E} and $-\mu\nabla B$ forces. The latter is absent in equation (11). We assume steady fields, and thus

describe the electric field in terms of ϕ , where $\mathbf{E} = -\nabla\phi$, giving

$$E_{\parallel} = -\frac{\partial \phi}{\partial \ell} \quad (12)$$

[14] The magnetospheric electrons are assumed to be perfectly trapped, and are described separately via an isotropic Maxwellian distribution function given by

$$f_M = n_M \left(\frac{m}{2\pi kT} \right)^{\frac{3}{2}} \exp\left(-\frac{1}{kT} \left(\frac{m}{2} (v_{\parallel}^2 + v_{\perp}^2) - e\phi \right) \right) \quad (13)$$

where n_M is the Maxwellian electron number density at ℓ_0 , kT is the magnetospheric electron thermal energy and ϕ is the potential variation along the field line between ℓ_0 and ℓ . Thus $\phi(\ell_0) = 0$ and we denote $\phi(\ell_m) = \phi_m$.

[15] We obtain the following expressions for the electron number density (n) and field-aligned current (j) by integrating the total distribution function $f = f_i + f_M$ over perpendicular and parallel velocity space:

$$\frac{n(\ell)}{B(\ell)} = \int_{-\infty}^{\infty} F(\ell, v_{\parallel}) dv_{\parallel} + \frac{n_M}{B(\ell)} \exp\left[\frac{e\phi}{kT} \right] \quad (14)$$

$$\frac{j(\ell)}{B(\ell)} = -e \int_{-\infty}^{\infty} v_{\parallel} F(\ell, v_{\parallel}) dv_{\parallel} \quad (15)$$

3. Downward Current Solution

3.1. Model Overview

[16] We begin by giving a basic overview of the model and important locations which arise from it, to orientate the reader through the calculations which follow. Figure 2 shows the setup of the model, and the important locations

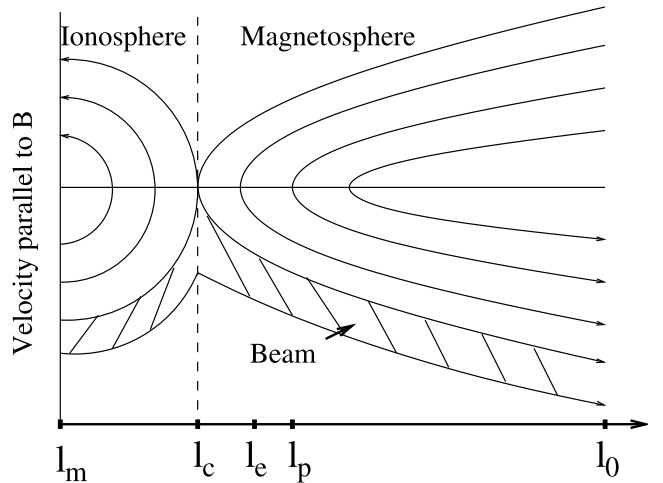


Figure 2. Diagram showing three electron populations: mirroring magnetospheric electrons, ionospheric electrons trapped by a small ambipolar electric field, and the beam. This diagram is not to scale; the magnetospheric population is much more energetic (~ 1 keV) than that in the ionosphere (~ 1 eV). Key locations in the model are: ℓ_m , the base of the F region; ℓ_c , the ionospheric trapping point; ℓ_e , the point where E_{\parallel} has its largest amplitude; ℓ_p , the location of the B/n peak; and ℓ_0 , a distant reference point in the magnetosphere. This figure is for the Northern Hemisphere.

along the flux tube calculated from the model. We consider a converging flux tube, where ℓ_m is the point at the base of the ionospheric F region and ℓ_0 is a distant point in the magnetosphere whose exact location is not important. We take the magnetic field and ion number density profiles given in equations (1) and (6) respectively, where we are free to choose B_0 , n_0 , n_m and h , and define the anti-earthward electron populations at ℓ_m and the earthward population at ℓ_0 . The flux tube naturally divides into two regions separated by ℓ_c , the ionospheric electron trapping point contained within the F region. The ionospheric electron population is mostly trapped earthward of ℓ_c , in the region $\ell_c < \ell < \ell_m$ since the solution to the Vlasov equation produces a small ambipolar potential in this region. A small beam of the most energetic ionospheric electrons, although slowed by this ambipolar electric field, manages to escape into the magnetosphere. It penetrates the magnetospheric electron population, taken to be a mirroring Maxwellian, in the region $\ell_0 < \ell < \ell_c$, where it is energized to carry the required downward current. Following *Temerin and Carlson* [1998], we assume that a negligible fraction of the Maxwellian magnetospheric electrons penetrates beyond ℓ_c , and that the contribution of these electrons to the current is also negligible (see Appendix B). The B/n peak is located at ℓ_p and is determined by the equilibrium model, and ℓ_e , the point where E_{\parallel} maximizes, is found to be located earthward of this peak, within three density scale heights.

3.2. Boundary Conditions and Constraints

[17] We impose an ionospheric boundary condition on $F(\ell, v_{\parallel})$ at ℓ_m : we take a top-hat distribution such that $F(\ell_m, v_{\parallel}) = F_1$, $-a_m - \varepsilon \leq v_{\parallel} \leq a_m$, where a_m corresponds to the ionospheric electron distribution thermal velocity width. The section $-a_m \leq v_{\parallel} \leq a_m$ corresponds to the trapped ionospheric population, and the component given by $-a_m - \varepsilon \leq v_{\parallel} < -a_m$ forms the current-carrying beam. We also impose a magnetospheric boundary condition such that $f = F_2$ at ℓ_0 for the mirroring Maxwellian population.

[18] Although the F region of the ionosphere defined in terms of ion density extends well above ℓ_c , this location is a natural mathematical dividing line in our model between the trapped ionospheric population and the mirroring Maxwellian where solutions must be matched, so we refer to the region $\ell_c < \ell < \ell_m$ as the ‘‘ionosphere,’’ and $\ell_0 < \ell < \ell_c$ as the ‘‘magnetosphere.’’

[19] We assume that the ion profile remains unchanged in time, and we keep the plasma quasi-neutral by equating the total electron number density to that of the ions, given in equation (6). We also impose current continuity on the model, i.e., $\nabla \cdot \mathbf{j} = \mathbf{0}$, which can be expressed as

$$\frac{j(\ell)}{B(\ell)} = \frac{j_m}{B_m} \quad (16)$$

where j_m and B_m are the current density and magnetic field strength at ℓ_m . Hence $B/n \propto$ the mean electron drift speed [Swift, 1975], giving a measure of the electron speed needed to carry the current in our model. We also make use of Liouville’s theorem in the formulation of our equations, which states that a distribution function is constant on an electron trajectory, as given in equation (7).

3.3. Ionospheric Equation

[20] The total energy of an ionospheric electron, W_0 , can be expressed as

$$\frac{W_0}{m} = \frac{v_{\parallel}^2}{2} - \Phi(\ell) \quad (17)$$

where $\Phi(\ell) = e\phi(\ell)/m$, $\phi(\ell)$ is the electric potential variation along the field line, and v_{\parallel} is the parallel electron velocity. If we know that an electron has a speed $v_{\parallel m}$ at ℓ_m , where $\Phi = \Phi_m$, then we can determine its speed at any other point since

$$\frac{v_{\parallel m}^2}{2} - \Phi_m = \frac{v_{\parallel}^2(\ell)}{2} - \Phi(\ell) \quad (18)$$

giving

$$v_{\parallel}(\ell) = \pm \sqrt{v_{\parallel m}^2 + 2\Delta\Phi(\ell)} \quad (19)$$

where $\Delta\Phi(\ell) = \Phi(\ell) - \Phi(\ell_m) = \Phi(\ell) - \Phi_m$, the change in normalized potential. Thus with $\Delta\Phi(\ell_c) = \Delta\Phi_c = -a_m^2/2$, we trap all of the ionospheric electrons except the current-carrying beam component with $-a_m - \varepsilon \leq v_{\parallel m} < -a_m$. At an arbitrary point between ℓ_m and ℓ_c , an electron with speed $-(a_m + \varepsilon)$ at ℓ_m will map to $v_{\parallel}(\ell) = -\sqrt{(a_m + \varepsilon)^2 + 2\Delta\Phi(\ell)}$. Electrons with $-a_m \leq v_{\parallel m} \leq 0$ are turned around between ℓ_m and ℓ_c and return to ℓ_m . So, an electron with speed a_m at ℓ_m will map to $v_{\parallel}(\ell) = \sqrt{a_m^2 + 2\Delta\Phi(\ell)}$. Thus, by Liouville’s theorem, the distribution at each point is a top-hat distribution such that $F = F_1$, $-\sqrt{(a_m + \varepsilon)^2 + 2\Delta\Phi} \leq v_{\parallel} \leq \sqrt{a_m^2 + 2\Delta\Phi}$. So, we can equate the electron and ion number densities in the ionosphere to obtain

$$\frac{n(\ell)}{B(\ell)} = F_1 \left(\sqrt{(a_m + \varepsilon)^2 + 2\Delta\Phi} + \sqrt{a_m^2 + 2\Delta\Phi} \right) \quad (20)$$

3.4. Magnetospheric Equation

[21] The magnetospheric equation contains a term corresponding to the mirroring isotropic Maxwellian population, and another corresponding to the emerging beam. The Maxwellian population gives a number density of $F_2 \exp(e\phi/kT)$. The only ionospheric electrons to emerge above ℓ_c are those with velocities in the range $-a_m - \varepsilon \leq v_{\parallel m} < -a_m$ at ℓ_m , so, again using Liouville’s theorem, they contribute a number density divided by B of

$$\frac{n^*}{B} = F_1 \left(\sqrt{(a_m + \varepsilon)^2 + 2\Delta\Phi} - \sqrt{a_m^2 + 2\Delta\Phi} \right) \quad (21)$$

giving the relation for charge neutrality in the magnetosphere ($\ell_0 < \ell < \ell_c$) as

$$\frac{n(\ell)}{B(\ell)} = \frac{F_2}{B(\ell)} \exp\left(\frac{m}{kT}(\Delta\Phi + \Phi_m)\right) + F_1 \left(\sqrt{(a_m + \varepsilon)^2 + 2\Delta\Phi} - \sqrt{a_m^2 + 2\Delta\Phi} \right) \quad (22)$$

3.5. Evaluating Constants and Nondimensionalizing Equations

[22] We can use equation (15) for field-aligned current density to evaluate the constant F_1 in the ionospheric equation. Now, the trapped ionospheric electrons contribute no net current since the current carried by upflowing electrons is cancelled by corresponding downflowing ones. So, the only contribution to this current comes from the beam since the beam electrons have no downflowing counterparts. So, at ℓ_m , electrons contributing to the current are those with speeds of $-a_m - \epsilon \leq v_{\parallel m} < -a_m$. So,

$$\frac{j_m}{B_m} = -eF_1 \int_{-a_m - \epsilon}^{-a_m} v_{\parallel} dv_{\parallel} \quad (23)$$

[23] From this, we can deduce that

$$F_1 = \frac{j_m}{eB_m \epsilon (a_m + \frac{\epsilon}{2})} \quad (24)$$

[24] We can find the magnetospheric distribution function amplitude F_2 by evaluating the magnetospheric equation (22) at ℓ_0 , where $\Delta\Phi(\ell_0) = -\Phi_m$, the normalized potential at ℓ_m , giving us

$$F_2 = n_0 - F_1 B_0 \left(\sqrt{(a_m + \epsilon)^2 - 2\Phi_m} - \sqrt{a_m^2 - 2\Phi_m} \right) \quad (25)$$

[25] We wish to express the ionospheric and magnetospheric equations (20) and (22) in terms of dimensionless parameters. Now, using (14) and (24), we can write that

$$\frac{n_m}{B_m} = \frac{2j_m}{eB_m \epsilon} \quad (26)$$

[26] From this, we can deduce an expression for the beam width, ϵ :

$$\epsilon = \frac{2j_m}{n_m e} \quad (27)$$

[27] Thus, as the current density increases, so does the beam width, as more current-carrying electrons will be required; as the ionospheric number density increases, the beam width decreases proportionally to carry the same current.

[28] There are four characteristic electron speeds or energies in this model: a_m and ϵ , the ionospheric background and beam thermal velocity widths at ℓ_m ; kT , the thermal energy of the background magnetospheric population at ℓ_0 ; and $v^*(\ell_0) \approx -\sqrt{a_m^2 - 2\Phi_m}$, the parallel velocity of the beam at ℓ_0 . These four characteristic speeds and energies can be expressed succinctly in terms of three dimensionless ratios with which we may reformulate our equations. Firstly, we define $\alpha = \epsilon/(2a_m)$, the ratio of the beam width in velocity space to the trapped ionospheric population width, a_m . Thus, using equation (27),

$$\alpha = \frac{j_m}{n_m e a_m} \quad (28)$$

and α corresponds to a normalized current density. Now, we can use equations (21) and (24) to find a relation for n^* , the beam number density:

$$\frac{n^*}{B} = \frac{j_m}{eB_m \epsilon (a_m + \frac{\epsilon}{2})} \left(\sqrt{(a_m + \epsilon)^2 + 2\Delta\Phi} - \sqrt{a_m^2 + 2\Delta\Phi} \right) \quad (29)$$

and v^* , the average velocity of the beam, using equation (19):

$$v^* = -\frac{1}{2} \left(\sqrt{(a_m + \epsilon)^2 + 2\Delta\Phi} + \sqrt{a_m^2 + 2\Delta\Phi} \right) \quad (30)$$

[29] Now, the current density, j , can be expressed as

$$j(\ell) = -n^*(\ell) e v^*(\ell) \quad (31)$$

so $j_m \approx n_m^* e a_m$, where $n_m^* = n^*(\ell_m)$. Thus we can deduce that $\alpha \approx n_m^*/n_m$, the ratio of the beam number density to the total ionospheric electron number density at ℓ_m . For downward currents in the Northern Hemisphere, α is positive, and α typically lies in the range 10^{-5} – 10^{-3} . The second dimensionless parameter we introduce is

$$\eta = \frac{m a_m^2}{2kT} \quad (32)$$

representing the ratio of the kinetic energy of the ionospheric electron population to the thermal energy of the magnetospheric electron population. This again is a small parameter: ionospheric electron temperatures are generally ~ 1 eV, while magnetospheric electron temperatures can vary from ~ 100 eV to several keV. Thus η is typically of the order of 10^{-4} – 10^{-2} . The third, and final, normalized parameter we define relates to the electric potential difference, so that

$$\Delta\tilde{\Phi} = \Delta\Phi / (a_m^2/2) \quad (33)$$

and

$$\tilde{\Phi} = \frac{2e\phi}{m a_m^2} \quad (34)$$

[30] Thus, substituting the average beam velocity v^* into equation (18), $\Delta\tilde{\Phi} \approx v^{*2}(\ell)/a_m^2 - 1$. Using these dimensionless parameters, we obtain the nondimensionalized equations for the ionosphere and magnetosphere respectively:

$$\frac{n(\ell)}{B(\ell)} \Big/ \frac{n_0}{B_0} = A \left(\sqrt{(1+2\alpha)^2 + \Delta\tilde{\Phi}} + \sqrt{1+\Delta\tilde{\Phi}} \right) \quad (35)$$

$$\frac{n(\ell)}{B(\ell)} \Big/ \frac{n_0}{B_0} = A \left(\sqrt{(1+2\alpha)^2 + \Delta\tilde{\Phi}} - \sqrt{1+\Delta\tilde{\Phi}} \right) + \frac{B_0}{B(\ell)} (1-AC) \exp(\eta(\Delta\tilde{\Phi} + \tilde{\Phi}_m)), \quad (36)$$

where

$$A = \left(\frac{n_m}{n_0}\right) \left(\frac{B_0}{B_m}\right) \frac{1}{2(1+\alpha)}. \quad (37)$$

and

$$C = \sqrt{(1+2\alpha)^2 - \tilde{\Phi}_m} - \sqrt{1 - \tilde{\Phi}_m} \quad (38)$$

[31] The magnetospheric equation (36) can be written as $n_{tot} = n^* + n_{mag}$ i.e., the total electron number density in the region $\ell_0 < \ell < \ell_c$ is the sum of the beam and Maxwellian number densities. In equations (36) and (38), $\tilde{\Phi}_m$ corresponds to the total potential difference across the field line. For downward currents, $\tilde{\Phi}_m$ is negative, so the total potential increase along the field line is given by $-\tilde{\Phi}_m$.

4. Results

[32] We can solve equations (35) and (36) numerically to find the potential variation along the field line, and the total potential increase along the field line, $-\tilde{\Phi}_m$. This is the current-voltage relation or Ohm's Law for the downward auroral current for an assumed fixed ion density profile. The solution for $\Delta\tilde{\Phi}$ is multivalued in the magnetosphere, but only the continuous, monotonically increasing solution satisfies our boundary conditions [see *Temerin and Carlson, 1998*]. We tested our model against the example given in *Temerin and Carlson [1998]*. We chose our boundary conditions (at ℓ_m) and our equilibrium such that their boundary conditions imposed at ℓ_c were satisfied, and successfully reproduced their result. For details, see Appendix A.

[33] Figure 3 shows a typical example for a current density at ℓ_m of $5 \mu\text{Am}^{-2}$, and ionospheric and magnetospheric electron temperatures of 1 eV and 1 keV respectively. Firstly, a small ambipolar electric field traps most of the ionospheric electrons below $s = \ell_m - \ell = 0.083 R_E$, and is shown in the enlarged plot of Figure 3b. In the magnetosphere, there is a monotonic increase in $\Delta\tilde{\Phi}$ with a localized acceleration region, which in this case extends from 0.2 to 0.6 R_E . This increase in potential in the magnetosphere performs two tasks in this model.

[34] At altitudes immediately above ℓ_c , the electrons are predominantly ionospheric upward beam electrons. In this region, which is below the B/n peak, the ion number density profile decays exponentially with altitude, whereas the current density $j \propto B \propto 1/r^3$ decays more slowly. Since n^* is approximately equal to the ion number density here, the beam speed needs to increase by equation (31) to carry the required current, and the potential increase is required to accelerate the electrons, increasing v^* . At higher altitudes, the potential increase not only accelerates the beam, but also has an effect on the mirroring magnetospheric electron population. The increasing magnetic field strength experienced by magnetospheric electrons as they travel earthward does mirror some, but the existence of a large potential barrier has the effect of excluding almost all of them from the ionospheric ambipolar region. This is advantageous, as

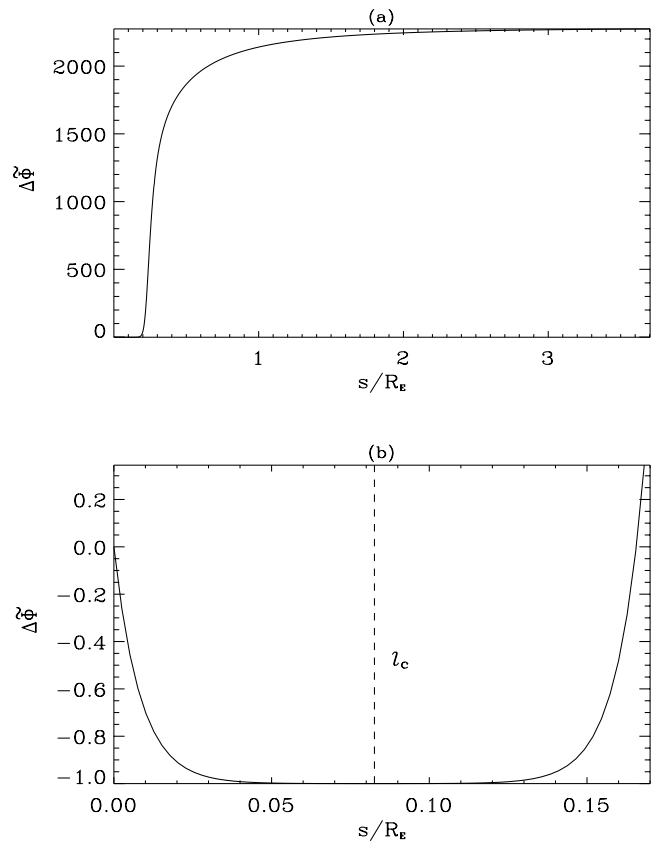


Figure 3. The variation of normalized potential, $\Delta\tilde{\Phi}$, with $s = \ell_m - \ell$ over (a) 4 Earth radii, showing the acceleration region between 0.2 and 0.6 R_E , and (b) 0.17 Earth radii, showing the small ambipolar electric field which traps the majority of the ionospheric electrons to within 0.083 R_E , or 530 km, of ℓ_m . In this example, $\alpha = 5 \times 10^{-5}$, corresponding to a current density at ℓ_m of $5 \mu\text{Am}^{-2}$, and $\eta = 10^{-3}$, corresponding, say, to an ionospheric electron temperature of 1 eV, and a magnetospheric electron temperature of 1 keV. In this case, the total potential drop along the field line is found to be 2.28 kV.

obviously any electrons which do enter that region will precipitate and form a counterstreaming beam, neglected in this calculation. The effect is negligible in the vast majority of cases, decreasing with increasing α (or current density) or η (see Appendix B).

4.1. Ionospheric Trapping Point, ℓ_c

[35] One property that emerges naturally from this model is the ionospheric trapping point, ℓ_c , the point earthward of which all ionospheric electrons except those forming the beam are trapped, and where the beam emerges from the ionosphere into the magnetosphere. At ℓ_c , electrons with $v_{||m} = -a_m$ at ℓ_m are slowed to $v_{||} = 0$. Substituting these values into equation (19), and using equation (33), we find that $\Delta\tilde{\Phi} = -1$ at ℓ_c , so we can substitute this into the ionospheric equation (35) to obtain the relation

$$\left(\frac{n_c}{B_c} / \frac{n_0}{B_0}\right) = \left(\frac{n_m}{n_0}\right) \left(\frac{B_0}{B_m}\right) \sqrt{\frac{\alpha}{1+\alpha}} \quad (39)$$

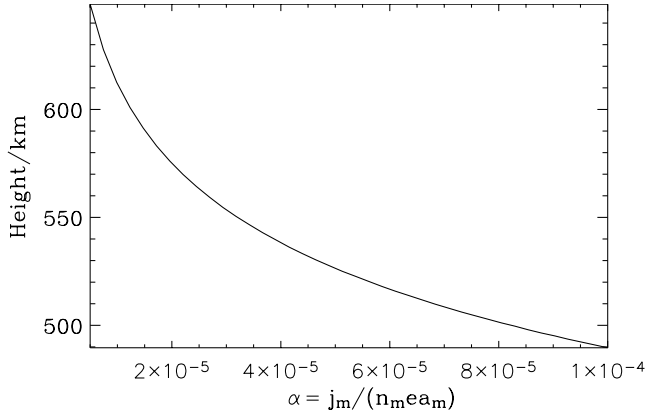


Figure 4. Variation of ionospheric trapping point ℓ_c with α .

[36] For $\alpha \ll 1$, this reduces to

$$\left(\frac{n_c}{B_c} / \frac{n_0}{B_0}\right) = \left(\frac{n_m}{n_0}\right) \left(\frac{B_0}{B_m}\right) \sqrt{\alpha} \quad (40)$$

[37] Thus, for a given α , we can find n_c/B_c , and then use the form of B/n shown in Figure 1 to find the height to which this corresponds. There will always be two possible heights, one before and one after the B/n peak, but ℓ_c always lies earthward of this. Figure 4 shows that typical ionospheric trapping points obtained from our model range from 500–650 km. It is interesting to note that the location of ℓ_c is unaffected by η , i.e., by the magnetospheric electron temperature for a given value of a_m .

[38] Substituting equation (28) into equation (40), we can see that

$$\left(\frac{n_c}{B_c} / \frac{n_0}{B_0}\right) = \frac{B_0}{B_m} \sqrt{\frac{j_m n_m}{e a_m n_0^2}} \quad (41)$$

[39] So, as the ionospheric temperature a_m increases, n_c/B_c decreases, giving a higher ionospheric trapping point, while as the ionospheric number density n_m or current density j_m increase, so does n_c/B_c , implying a lower altitude ionospheric trapping point. This latter point agrees with the observation made by *Temerin and Carlson* [1998] that for larger currents the ambipolar field must go to zero at larger ionospheric densities (i.e., at lower altitudes) to supply sufficient current-carrying electrons.

[40] At ℓ_c , the beam number density n^* has a significant peak, as by equation (31), the ambipolar electric field slows the ionospheric population so much that v^* dips to its lowest value, and a large increase in n^* is necessary to maintain the current around this point.

4.2. Location of Maximum E_{\parallel} , ℓ_e

[41] There is a maximum in the parallel electric field, $E_{\parallel}(\ell_e) = E_{\parallel\max}$, which occurs between ℓ_c and ℓ_p , near the start of the acceleration region: it is needed to provide acceleration over a scale comparable to the density scale height. Using equations (12) and (34), we know that

$$E_{\parallel} = -\frac{m a_m^2}{2e R_E} \frac{\partial \Delta \tilde{\Phi}}{\partial (\ell/R_E)} \quad (42)$$

[42] From this, we can define a normalized parallel electric field, \tilde{E}_{\parallel} , such that

$$\tilde{E}_{\parallel} = \frac{2e R_E}{m a_m^2} E_{\parallel} = -\frac{\partial \Delta \tilde{\Phi}}{\partial (\ell/R_E)} \quad (43)$$

[43] This electric field can be found numerically, and a typical result is shown in Figure 5. Figure 6 shows the variation of $E_{\parallel\max}$ with α and η , which extends up to 10 mV m^{-1} , for an ionospheric electron temperature of 1 eV. As the current density, or α , increases, more acceleration is needed; therefore $E_{\parallel\max}$ increases.

[44] ℓ_e is located beyond the ionospheric trapping point, ℓ_c , and within three density scale heights of the B/n peak. As the current density increases, ℓ_e is found to move earthward, as quasi-neutrality dictates that acceleration is needed closer to ℓ_c . As the magnetospheric electron temperature increases (causing a decrease in η), ℓ_e moves closer to the B/n peak, indicating the importance of the electric field for reflecting magnetospheric electrons to make room for the current-carrying ionospheric beam electrons.

4.3. Width of Acceleration Region, Ω

[45] The distance over which the potential increase occurs depends on the parameters α and η . In order to get an idea of the trends involved, we define the acceleration region to start at the point where $\Delta \tilde{\Phi} = 0$ beyond ℓ_c (since the increase from ℓ_c , where $\Delta \tilde{\Phi} = -1$, to the point where $\Delta \tilde{\Phi} = 0$ is gradual) and to end where $\Delta \tilde{\Phi} = -0.8 \tilde{\Phi}_m$. We define Ω to be the distance between these two points, giving a measure of the width of the acceleration region. This parameter gives an idea of how localized the potential increase is.

[46] The results are shown in Figure 7. As the current density increases, Ω decreases, despite the fact that the overall potential increase gets larger: this implies a much smaller, more concentrated acceleration region surrounding the B/n peak. As the magnetospheric electron temperature increases (indicating a decrease in η), Ω increases too. This implies that the acceleration region is not so concentrated.

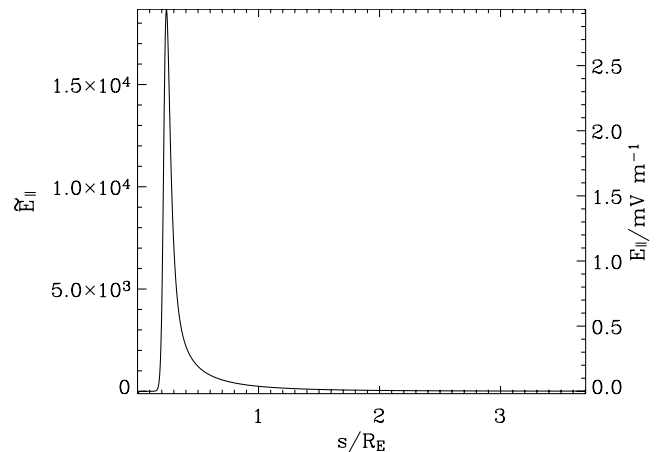


Figure 5. Variation of \tilde{E}_{\parallel} along the field line for $\alpha = 5 \times 10^{-5}$ and $\eta = 10^{-3}$, showing the maximum of \tilde{E}_{\parallel} , which occurs between ℓ_c and the B/n peak, at $s/R_E = 0.240$, or 1530 km. The form of E_{\parallel} is shown for an ionospheric electron temperature of 1 eV, and $E_{\parallel\max}$ is 2.93 mV m^{-1} .

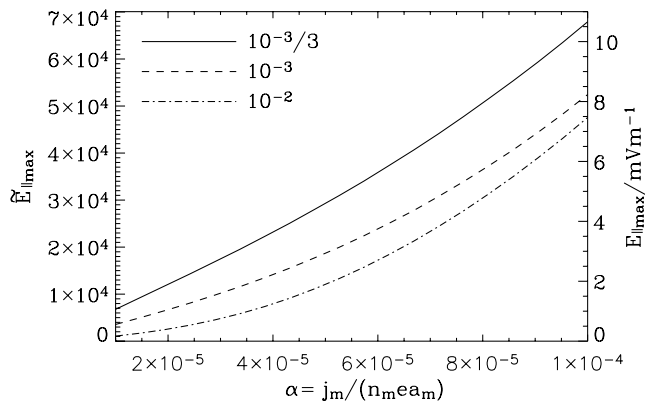


Figure 6. Variation of the maximum \tilde{E}_{\parallel} with α and three different values of η . $E_{\parallel\max}$ is shown in mV m^{-1} for an ionospheric electron temperature of 1 eV. In this case, the magnetospheric electron temperatures are 3 keV (solid curve), 1 keV (dashed curve), and 100 eV (dot-dashed curve).

Much of the energization will still occur over a small distance around the B/n peak, but some of it extends further into the magnetosphere. This performs a useful role: since the magnetospheric Maxwellian electrons are now more energetic, the presence of a prohibitive potential difference in the magnetosphere has the effect of mirroring more of these electrons so that they do not penetrate too deeply into the acceleration region. This will enable matching of the electron and ion number densities along the field line.

4.4. Significance of B/n Peak

[47] The ion number density profile chosen in this model is obviously vital to the solution of equations (35) and (36) since the total electron density must match this profile to satisfy quasi-neutrality. Hence it would be reasonable to think that altering the ion number density must have an effect upon $\tilde{\Phi}_m$, the total potential difference along the field line. However, it turns out that only the number density

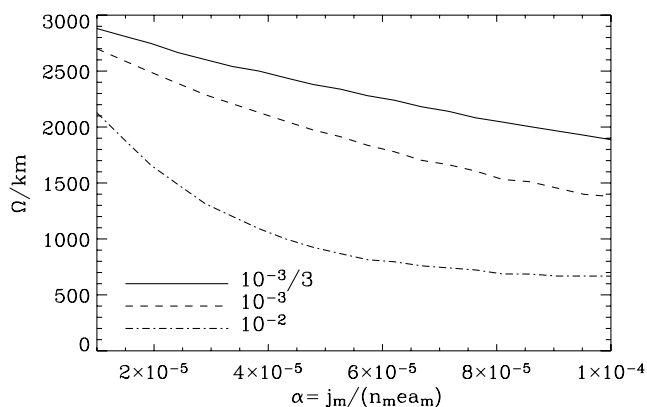


Figure 7. Variation of the width of the acceleration region with α and three different values of η . Assuming an ionospheric electron temperature of 1 eV, these η values correspond to magnetospheric electron temperatures of 3 keV (solid curve), 1 keV (dashed curve), and 100 eV (dot-dashed curve).

in the vicinity of the B/n peak is vital to the overall solution of the equations, and hence, to $\tilde{\Phi}_m$.

[48] To illustrate this, we altered the number density profile given in equation (6) on either side of the B/n peak, defining a new density profile, n_1 . The alteration is shown in Figure 8, where $\delta n = |n_1 - n|$, the difference between the two number density profiles. The only constraint when changing the ion density profile is that it is necessary to preserve the single peak in the B/n curve and the boundary values at ℓ_m and ℓ_0 . If the B/n curve has multiple peaks, the potential profile obtained from the model is no longer monotonic in the magnetosphere, giving an unphysical result. This constraint allows for large changes in number density earthward of the B/n peak, but is more limiting beyond it. Hence $\delta n/n \sim 10^{-3}$ is the largest change possible beyond the B/n peak since n/n_0 only decreases from 1.04 to 1.00 between the B/n peak and ℓ_0 . It is somewhat surprising that the total potential drop, $\tilde{\Phi}_m$, calculated for the original density profile and the modified one are identical to the accuracy of our numerical solution (at least 5 significant figures).

[49] The change to the number density profile beyond the B/n peak may seem very small, suggesting that no significant change in $\tilde{\Phi}_m$ will result. However, when we alter the number density at, rather than either side of, the B/n peak such that $\delta n/n \sim 10^{-3}$ in this region, we do obtain a significant relative change in $\tilde{\Phi}_m \sim 10^{-3} - 10^{-2}$. These results demonstrate that the properties of the small region surrounding the B/n peak (\sim a few density scale heights) are solely responsible for determining $\tilde{\Phi}_m$.

5. Total Potential Difference, $\tilde{\Phi}_m$

5.1. Properties of $\tilde{\Phi}_m$

[50] Figure 9 shows the variation of $\tilde{\Phi}_m$ with α and η for scale heights of 50 and 200 km and n_m/n_0 values of 5×10^4 and 10^6 . These range over typical values, and reveal various properties of $\tilde{\Phi}_m$. In general, as α increases, implying a higher current density, so does the potential difference, $\tilde{\Phi}_m$.

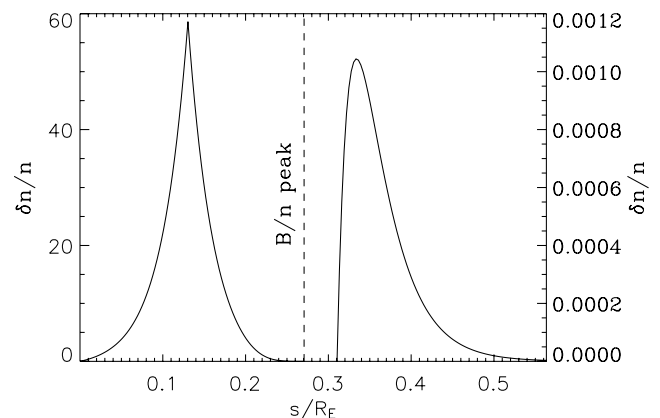


Figure 8. Alteration to ion number density. This alteration can be much larger on the earthward side of the B/n peak while still retaining a single B/n peak, while the alteration beyond the B/n peak is more restricted by this condition. This change in density profile results in no change to $\tilde{\Phi}_m$, illustrating the importance of the region surrounding the B/n peak to finding this total potential difference.

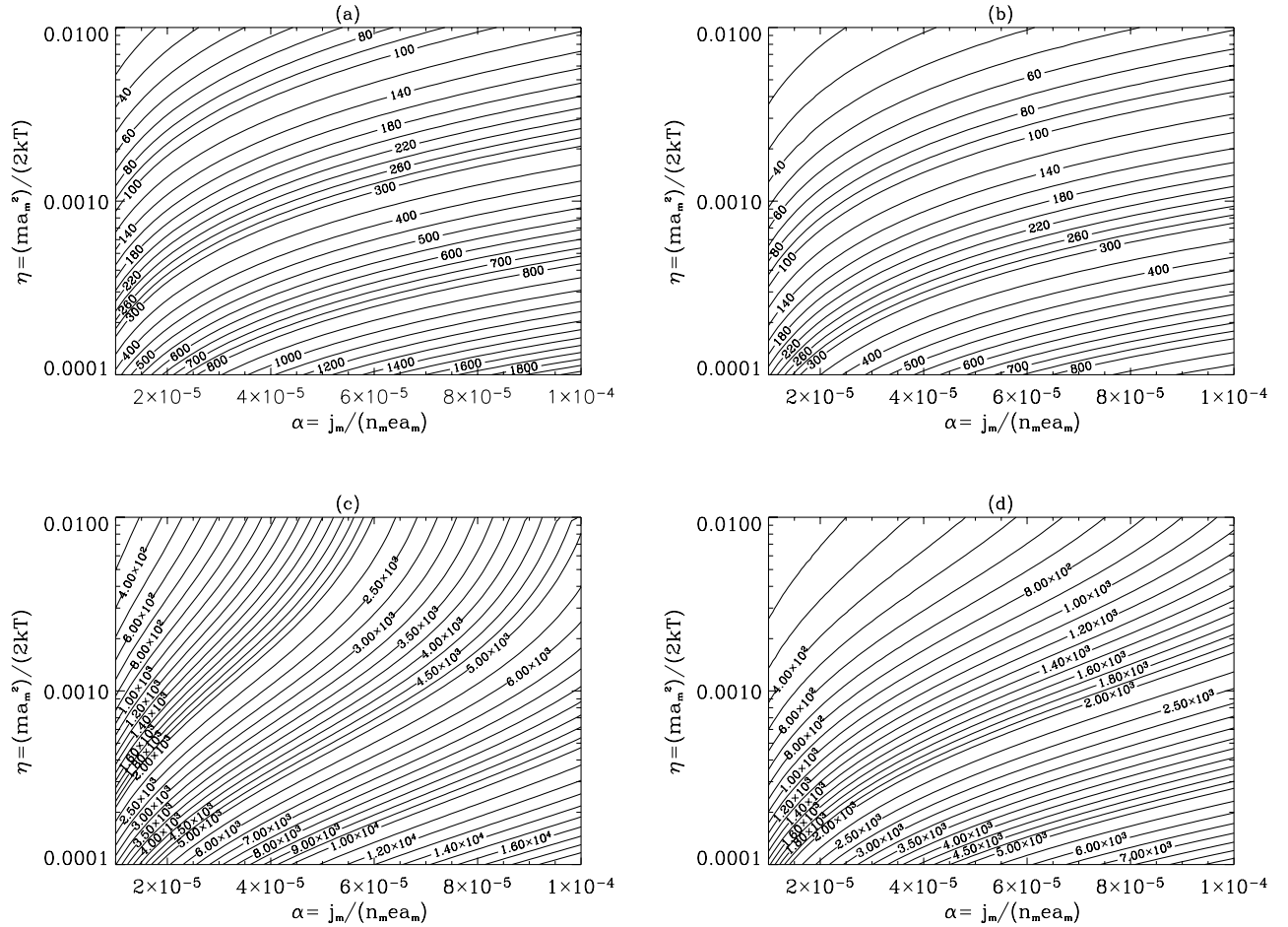


Figure 9. Four contour plots of $-\tilde{\Phi}_m$, the total potential increase along the field line, against α and η , for different ion number densities and scale heights; (a and b) $n_m/n_0 = 5 \times 10^4$ and (c and d) 10^6 . Figures 9a and 9c are for a scale height, h , of 50 km, while Figures 9b and 9d are for 200 km.

$\tilde{\Phi}_m$ also increases as the difference in electron ionospheric and magnetospheric temperatures increases, corresponding to a decrease in η . Comparisons between the contour plots also show that increasing the ion scale height, h , decreases $\tilde{\Phi}_m$, while increasing the ion number density, n_m/n_0 , results in an increase in $\tilde{\Phi}_m$. The contour plots can be used to determine the total potential increase for a given downward current event as follows.

5.1.1. Step 1

[51] Choose the equilibrium parameters of the event: the magnetospheric thermal electron energy (kT), the ionospheric electron thermal energy ($m_e a_m^2/2$), the ion number density at the base of the F region (n_m) and at ℓ_0 in the magnetosphere (n_0), the ion scale height (h), and the current density at the base of the F region (j_m). If you know the current density at a particular altitude, use the current continuity equation (16) to map this down to j_m .

5.1.2. Step 2

[52] Calculate the dimensionless parameters α and η from equations (28) and (32) respectively.

5.1.3. Step 3

[53] Use your α and η values to read off the required potential increase from the contour plot which has parameters closest to yours. Alternatively, if your value for h or n_m/n_0 lies between the ones we have shown, then read off

two values of $\tilde{\Phi}_m$ and extrapolate between them. For example, if $h = 100$ km and $n_m/n_0 = 10^6$, then read off the required $\tilde{\Phi}_m$ values from both of the plots with $n_m/n_0 = 10^6$, giving $\tilde{\Phi}_m(50)$ and $\tilde{\Phi}_m(200)$ for scale heights of 50 and 200 km respectively. Then interpolate, so that

$$\tilde{\Phi}_m(100) = \frac{2}{3}\tilde{\Phi}_m(50) + \frac{1}{3}\tilde{\Phi}_m(200) \quad (44)$$

[54] This gives an estimate of $\tilde{\Phi}_m(100)$, the total potential increase for a scale height of 100 km.

5.2. Comparison With Data

[55] In order to test the validity of this model, we compare the results that it gives with FAST data presented in the work of *Elphic et al.* [2000, Plate 1]. At the end of the first downward current phase (indicated by vertical dotted red lines starting at UT = 09:18), an inferred current density, j_{FAST} of $1.6 \mu\text{Am}^{-2}$ is observed at the altitude of FAST (second panel), and the associated electron energy is ~ 2 keV (fourth panel).

[56] Firstly, we need to calculate j_m using equation (16), noting that the altitude of FAST is ~ 4000 km. This gives us $j_m = 6.94 \mu\text{Am}^{-2}$. The electron energy spectra suggest that we have typical ionospheric and magnetospheric electron

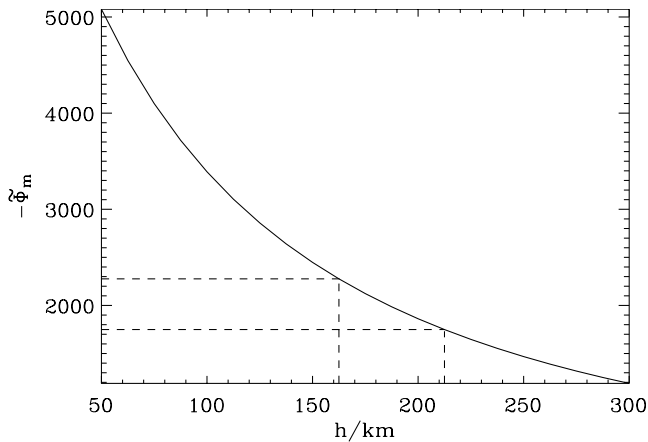


Figure 10. Variation of $\tilde{\Phi}_m$ with h for $j_m = 6.94 \mu\text{Am}^{-2}$ and $j_{FAST} = 1.6 \mu\text{Am}^{-2}$ at an altitude of 4000 km. The data show $\tilde{\Phi}_m \sim 2$ kV, implying an ion scale height of 160–210 km.

temperatures of 1 eV and 1 keV respectively. Assuming $n_m/n_0 = 10^6$, we find that $\alpha = 7.30 \times 10^{-5}$ from equation (28) and $\eta = 10^{-3}$ from equation (32).

[57] The ion scale height h can vary due to several factors, including the ion temperature, and the presence of additional features in the downward current region such as ion conics. We can use the information above to infer the value of h in this case. In Figure 10, we compute $\tilde{\Phi}_m$ for ion scale heights varying from 50 to 300 km. For $\tilde{\Phi}_m \sim 2$ kV, this corresponds to $h \sim 160$ –210 km, which is a very reasonable range.

6. Discussion and Conclusions

[58] We have presented a distribution function solution for ionospheric electrons accelerated into the magnetosphere to form an upflowing beam which carries the downward FAC coupling both regions. This formulation is advantageous as it is possible to isolate the different electron populations involved: the trapped ionospheric population, the mirroring Maxwellian magnetospheric population, and the current-carrying beam. The ionospheric population (except the beam) is found to be trapped below ℓ_c , which lies earthward of the B/n peak at altitudes of 300–700 km. Above this, the beam emerges into the magnetosphere. E_{\parallel} maximizes beyond ℓ_c , within three density scale heights of the B/n peak; this is near the beginning of the acceleration region, which extends for between 500 and 3000 km around the B/n peak.

[59] We have demonstrated that, for given boundary conditions, the exact form of the ion number density profile is unimportant except within a few density scale heights around the B/n peak. It is the properties of this region which define the overall solution, including $\tilde{\Phi}_m$. This highlights that the properties of this model are general, and not just confined to the specific density profiles used in this paper. Different density profiles could include those produced by the presence of ion conics trapped earthward of the acceleration region, as discussed by *Temerin and Carlson* [1998], which have the effect of increasing the ion number density along the field line, thus increasing the ion scale height.

These ion conics will modify the ion distribution. The ion scale height, h , and ion number density, n_m/n_0 , are the main factors which affect the location of the B/n peak. Studies of FAST data by *Cattell et al.* [2004] and *Carlson et al.* [1998] show that upward accelerated electron beams are much more prevalent in the winter or midnight sectors than they are in regions where the ionosphere is sunlit. This implies a strong dependence on scale height.

[60] From observations [e.g., *Ergun et al.*, 2003], it is apparent that the acceleration in the downward current region can occur over a very small distance (a double layer). In this case, it is obvious that the change in potential occurs over a very small region, which could be thought of as an extreme version of our model with a compacted acceleration width. This can be achieved via a sharp fall (or sudden change) in ion number density at the required altitude. *Temerin and Carlson* [1998] used such a profile, and obtained a sharp increase in potential. This type of feature in the ion density could evolve from the motion of ions along the field line in a time-dependent model. This is not dissimilar to our model, where the result is also determined by the properties of a very small region around the B/n peak, which in the compacted case would occur within the double layer. Thus the results should not be radically different, except that more of the potential increase would occur over a shorter distance: a feature seen very clearly in our reproduction of $\phi(B)$ for *Temerin and Carlson's* [1998] density profile (see Appendix A).

[61] Although observations of double layers show that they may move upward with the ion acoustic speed (a few 10s of km s^{-1} [*Andersson et al.*, 2002]), this is small compared to the electron speeds, suggesting that the quasi-steady potential viewpoint presented in our calculation is still appropriate. Besides neglecting the evolution of ions, we also do not address the stability of the beam and subsequent thermalization, including any necessary additional energization that is required. Simulations by *Ergun et al.* [2003] show that there is a rich variety of physics operating here. Their results also show that about 80% of the potential drop is associated with stable acceleration as described in our paper, with the remainder occurring in a turbulent thermalizing region downstream.

[62] Typical values for $\tilde{\Phi}_m$ obtained from this model are consistent with those obtained by *Temerin and Carlson* [1998], and range from several 100 V to a few kV. This agrees very well with typically observed values, and we have shown good agreement with a specific data set from *Elphic et al.* [2000]. It will be worthwhile to compare results from our model more closely with observational data over a wider range of conditions to check validity.

Appendix A: Comparison With *Temerin and Carlson* [1998]

[63] Since our model is an extension of that by *Temerin and Carlson* [1998], we tested our model using the example they cite, the results of which are given in their Figure 1. We used all of the same parameters, and an identical number density distribution. Our model starts at ℓ_m , the base of the F region, while the *Temerin and Carlson* model begins at ℓ_c . To compare with their model, we chose our boundary conditions and equilibrium between ℓ_m and ℓ_c such that

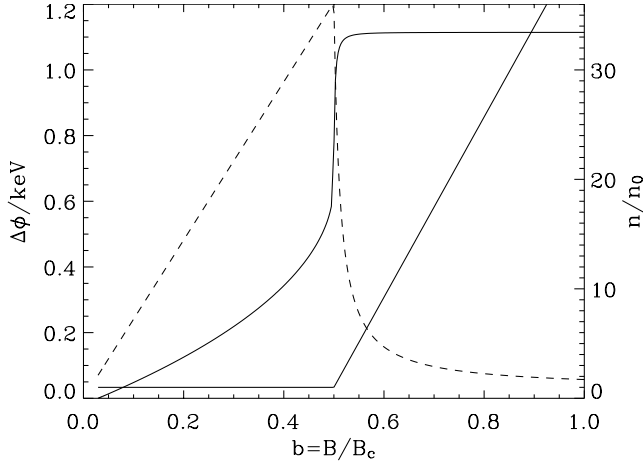


Figure A1. Our reproduction of the result in the work of *Temerin and Carlson* [1998, Figure 1]. Using all of their parameters and number density profile, we obtain $\tilde{\Phi}_m = -4073$, which gives a potential difference of 1.13 kV. The dashed plot is a scaled version of the B/n curve, $(B/n)/(250 B_0/n_0)$, which clearly shows that the B/n peak occurs at $b = 0.5$. Note the large E_{\parallel} (rapid change in $\Delta\phi$) which occurs where the density scale length is small (near the B/n peak).

our solution at ℓ_c coincides exactly with the boundary conditions that *Temerin and Carlson* imposed there.

[64] The field aligned coordinate used is $b = B/B_c$, where B_c represents the magnetic field strength at ℓ_c , and b extends from 0 (an idealized point in the magnetosphere) to 1 at ℓ_c . The number density is taken to be constant (1 cm^{-3}) between $b = 0$ and 0.5 , and increases linearly thereafter up to $b = 1$, at an altitude of 3000 km. We extend this linear increase to give $n_m = 2.23 \times 10^8 \text{ m}^{-3}$. The current density is taken to be $2.0 \text{ } \mu\text{Am}^{-2}$ at ℓ_c , and using the current continuity equation (16), we obtain $j_m = 6.39 \text{ } \mu\text{Am}^{-2}$.

[65] Using our exact relation at ℓ_c in equation (39), $\alpha = 0.572$. This is an unusually large value, and is due to the linear rather than exponential ion density profile. From this we can find that $a_m = 3.13 \times 10^5 \text{ ms}^{-1}$ from equation (28). This gives an ionospheric electron temperature of 0.278 eV, which, along with *Temerin and Carlson's* [1998] choice of a magnetospheric electron temperature of 1 keV, gives $\eta = 2.78 \times 10^{-4}$ from equation (32). Using our model, we obtain a normalized potential difference $\tilde{\Phi}_m = -4073$. From equation (34), this corresponds to an actual potential difference of 1.13 kV, identical to the value found by *Temerin and Carlson*. Our results are shown in Figure A1. We could have chosen a different extrapolated density for $\ell_c < \ell < \ell_m$ which would have given more typical values of n_m , α and η . What is important for the present comparison is that our values at ℓ_c match those of *Temerin and Carlson*.

Appendix B: Validity of Assumptions

[66] In this model, we assume that the magnetospheric number density is negligible at altitudes below ℓ_c , i.e., that no magnetospheric electrons penetrate into the ionosphere. In reality, since the distribution is Maxwellian, a few of the most energetic field-aligned magnetospheric electrons will be able to overcome the large potential barrier and penetrate

into the ionosphere, thus producing a downward magnetospheric electron population and reducing the net upward flux. It is possible to calculate the neglected current density and number density at ℓ_c and compare these with the beam current and number densities to check the validity of this assumption.

[67] The neglected current density, j_{\parallel}^u , can be found by integrating the Maxwellian electron distribution given in equation (13) over v_{\parallel} and v_{\perp} space as follows:

$$j_{\parallel}^u = -e \int_0^{\infty} \int_0^{\infty} v_{\parallel} f_M dv_{\parallel} 2\pi v_{\perp} dv_{\perp} \quad (\text{B1})$$

[68] Using the following integrals

$$\int_0^{\infty} v_{\perp} \exp\left(-\frac{m}{2kT} v_{\perp}^2\right) dv_{\perp} = \int_0^{\infty} v_{\parallel} \exp\left(-\frac{m}{2kT} v_{\parallel}^2\right) dv_{\parallel} = \frac{kT}{m} \quad (\text{B2})$$

and the fact that $\Delta\tilde{\Phi} = -1$ at ℓ_c , we obtain

$$j_{\parallel}^u = -en_0 \sqrt{\frac{kT}{2\pi m}} \exp(\eta(\tilde{\Phi}_m - 1)) \quad (\text{B3})$$

[69] Using the current continuity condition in equation (16), we know that $j_c = B_c j_m / B_m$, giving

$$\left| \frac{j_{\parallel}^u}{j_c} \right| = \frac{1}{2\alpha} \left(\frac{B_m}{B_c} \right) \left(\frac{n_0}{n_m} \right) \sqrt{\frac{1}{\pi\eta}} \exp(\eta(\tilde{\Phi}_m - 1)) \quad (\text{B4})$$

[70] Similarly, we can work out the ratio of number densities at ℓ_c . Here, the electron beam accounts for the total ionospheric electron number density. Thus rearranging equation (39)

$$\frac{n_c^*}{n_0} = \left(\frac{n_m}{n_0} \right) \left(\frac{B_c}{B_m} \right) \left(1 + \frac{1}{\alpha} \right)^{-1} \quad (\text{B5})$$

[71] The magnetospheric number density at ℓ_c is determined by substituting $\Delta\tilde{\Phi} = -1$ into the second (Maxwellian) term on the RHS of equation (36) to yield

$$\frac{n_c^{\text{mag}}}{n_0} = (1 - AC) \exp(\eta(\tilde{\Phi}_m - 1)) \quad (\text{B6})$$

where A and C are determined by equations (37) and (38) respectively. Thus we obtain the ratio

$$\frac{n_c^{\text{mag}}}{n_c^*} = (1 - AC) \left(\frac{n_0}{n_m} \right) \left(\frac{B_m}{B_c} \right) \sqrt{1 + \frac{1}{\alpha}} \exp(\eta(\tilde{\Phi}_m - 1)) \quad (\text{B7})$$

[72] Contour plots of the ratios in equations (B4) and (B7) are given in Figure B1. These reveal that the neglected number density at ℓ_c is always negligible compared to the beam number density for relevant values of α and η . The neglected current density, however, is sometimes significant: when α and η are both very small, the neglected current density is comparable to the beam number density,

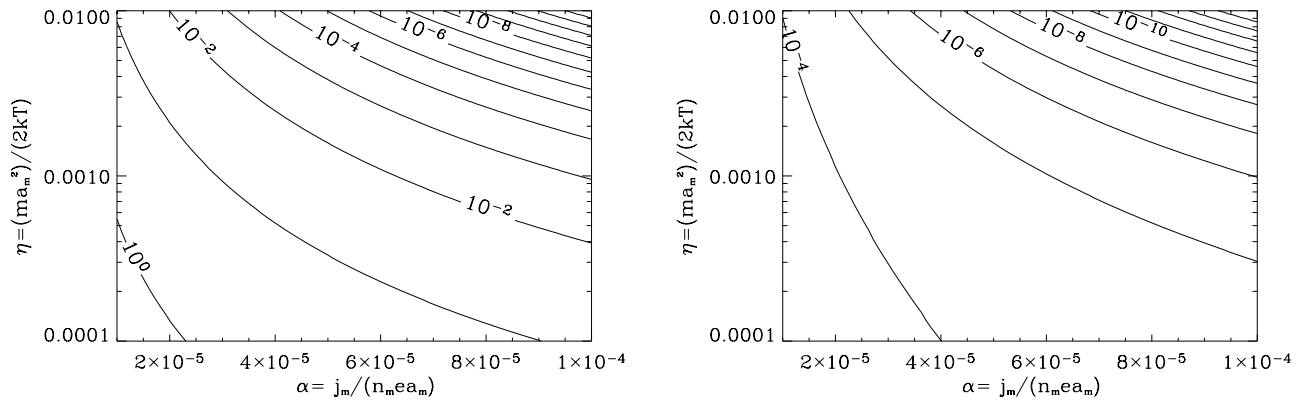


Figure B1. Contour plots showing (left) the ratio of neglected magnetospheric and beam current densities and (right) number densities at ℓ_c for $n_m/n_0 = 10^6$ and $h = 100$ km. These plots reveal that the beam number density is always much greater than the magnetospheric contribution. The current densities, however, can be comparable for very small values of α and η . As either of these parameters increases, so does the accuracy of our assumption.

but as either of these parameters increases (implying a larger beam current density or smaller difference between ionospheric and magnetospheric electron temperatures) the ratio becomes smaller, implying that the assumption becomes more accurate. These results make sense, as when j_m is small, j_c will also be small, so the magnetospheric component is more likely to yield a comparable upward current density. Also, a decrease in η implies an increase in magnetospheric electron temperature, so more energetic electrons will be able to overcome the potential barrier and contribute to an upward current at ℓ_c .

[73] **Acknowledgments.** Alexandra Cran-McGreehin's Ph.D. studies are being funded by the Carnegie Trust for the Universities of Scotland.

[74] Lou-Chuang Lee thanks one reviewer for the assistance in evaluating this paper.

References

- Andersson, L., R. E. Ergun, D. L. Newman, J. P. McFadden, C. W. Carlson, and Y.-J. Su (2002), Characteristics of parallel electric fields in the downward current region of the aurora, *Phys. Plasmas*, *9*, 3600.
- Carlson, C. W., et al. (1998), FAST observations in the downward auroral current region: Energetic up-going electron beams, parallel electric fields, and ion heating, *Geophys. Res. Lett.*, *25*, 2017.
- Cattell, C., J. Dombeck, W. Yusof, C. Carlson, and J. McFadden (2004), FAST observations of the solar illumination dependence of upflowing electron beams in the auroral zone, *J. Geophys. Res.*, *109*, A02209, doi:10.1029/2003JA010075.
- Chiu, Y. T., and M. Schultz (1978), Self-consistent particle and parallel electrostatic field distributions in the magnetospheric-ionospheric auroral region, *J. Geophys. Res.*, *83*, 629.
- Elphic, R., J. Bonnell, R. J. Strangeway, C. W. Carlson, M. Temerin, J. P. McFadden, R. E. Ergun, and W. Peria (2000), FAST observations of

- upward accelerated electron beams and the downward field-aligned current region, in *Magnetospheric Current Systems*, *Geophys. Monogr. Ser.*, vol. 118, edited by S. Ohtani et al., p. 173, AGU, Washington, D. C.
- Ergun, R. E., et al. (1998), FAST satellite observations of electric field structures in the auroral zone, *Geophys. Res. Lett.*, *25*, 2025.
- Ergun, R. E., C. W. Carlson, J. P. McFadden, F. S. Mozer, and R. J. Strangeway (2000), Parallel electric fields in discrete arcs, *Geophys. Res. Lett.*, *27*, 4053.
- Ergun, R. E., L. Andersson, C. W. Carlson, D. L. Newman, and M. V. Goldman (2003), Double layers in the downward current region of the aurora, *Nonlinear Proc. Geophys.*, *10*, 45.
- Jaspere, J. (1998), Ion heating, electron acceleration, and the self-consistent parallel electric field in downward current regions, *Geophys. Res. Lett.*, *25*, 3485.
- Marklund, G., L. Blomberg, C.-G. Fälthammar, and P. A. Lindqvist (1994), On intense diverging electric fields associated with black aurora, *Geophys. Res. Lett.*, *21*, 1859.
- Rönmark, K. (2002), The auroral current-voltage relation, *J. Geophys. Res.*, *107*(A12), 1430, doi:10.1029/2002JA009294.
- Stern, D. P. (1981), One-dimensional models of quasi-neutral parallel electric fields, *J. Geophys. Res.*, *86*, 5839.
- Swift, D. W. (1975), On the formation of auroral arcs and acceleration of auroral electrons, *J. Geophys. Res.*, *80*, 2096.
- Temerin, M., and C. W. Carlson (1998), Current-voltage relationship in the downward current region, *Geophys. Res. Lett.*, *25*, 2365.
- Vedin, J., and K. Rönmark (2004), A linear auroral current-voltage relation in fluid theory, *Ann. Geophys.*, *22*, 1719.
- Wright, A. N., and A. W. Hood (2003), Field-aligned electron acceleration in Alfvén waves, *J. Geophys. Res.*, *107*(A3), 1135, doi:10.1029/2002JA009551.

A. P. Cran-McGreehin and A. N. Wright, Mathematical Institute, University of St. Andrews, St. Andrews, Fife KY16 9SS, UK. (alex@mcs.st-and.ac.uk; andy@mcs.st-and.ac.uk)